

Thermo-Resistive Instability of Hot Planetary Atmospheres

Kristen Menou¹

ABSTRACT

The atmospheres of hot Jupiters and other strongly-forced exoplanets are susceptible to a thermal instability in the presence of ohmic dissipation, weak magnetic drag and strong winds. The instability occurs in radiatively-dominated atmospheric regions when the ohmic dissipation rate increases with temperature faster than the radiative (cooling) rate. The instability domain covers a specific range of atmospheric pressures and temperatures, typically $P \sim 3\text{--}300$ mbar and $T \sim 1500\text{--}2500$ K for hot Jupiters, which makes it a candidate mechanism to explain the dayside thermal “inversions” inferred for a number of such exoplanets. The instability is suppressed by high levels of non-thermal photoionization, in possible agreement with a recently established observational trend. We highlight several shortcomings of the instability treatment presented here. Understanding the emergence and outcome of the instability, which should result in locally hotter atmospheres with stronger levels of drag, will require global non-linear atmospheric models with adequate MHD prescriptions.

1. Introduction

A variety of gaseous exoplanets with strongly-forced atmospheres have been discovered by astronomers (e.g., Charbonneau 2009). These exoplanets, exemplified by the hot Jupiter class, receive extreme levels of irradiation from their stellar host and likely experience permanent day- and night-side forcing conditions, from being tidally-locked on very compact orbits. Observationally, two of the most interesting trends emerging from studies of well-characterized, transiting hot Jupiters have been the tendency for many such planets to exhibit radius inflation, well above expectations from standard planetary cooling models, and the inference that thermal excesses (inversions) are present on the dayside of some of the strongly-irradiated planets (see Deming & Seager 2009; Baraffe et al. 2010; Burrows & Orton 2010; Winn 2010 for reviews).

¹Department of Astronomy, Columbia University, 550 West 120th Street, New York, NY 10027

It has recently been proposed that hot, strongly-forced exoplanet atmospheres are the site of significant magnetic induction when fast, weakly-ionized atmospheric winds cross the pre-existing planetary magnetic field. This induction takes the form of magnetic drag acting to brake atmospheric winds and associated ohmic heating in the planetary atmosphere and interior (Batygin & Stevenson 2010; Perna, Menou & Rauscher 2010a,b; Menou 2012). While other mechanisms have been proposed, ohmic heating is currently one of the leading contenders to explain the inflated radii of hot Jupiters (Batygin et al. 2011; Laughlin et al. 2011; Menou 2012; Wu & Lithwick 2012).

In this letter, we explore the possibility that thermal inversions in hot Jupiter atmospheres are not caused by extra absorption of stellar light at altitude, as they have traditionally been interpreted (Hubeny et al. 2003; Fortney et al. 2006, 2008; Burrows et al. 2008; Madhusudhan & Seager 2010), but instead result from the same induction mechanism that may explain radius inflation. In this alternative interpretation, thermal inversions have their origin in a thermo-resistive instability that affects radiatively-dominated atmospheric regions under specific conditions of weak magnetic drag, strong ohmic dissipation and fast winds.

2. Thermo-Resistive Instability Criterion

Let us first establish the existence of a thermo-resistive instability under physical conditions relevant to hot exoplanet atmospheres.

Energy Equation – The energy equation satisfied by an atmosphere experiencing ohmic dissipation can be written

$$\rho C_p \frac{dT}{dt} = \rho C_p \left(\frac{\partial T}{\partial t} + \mathbf{v} \cdot \nabla T \right) = -\nabla \cdot \mathbf{F}_{\text{rad}} + Q_{\text{ohm}} = Q_{\text{rad}} + Q_{\text{ohm}},$$

where ρ is the mass density, C_p is the specific heat at constant pressure and Q_{ohm} is the volumic ohmic dissipation rate. In the last expression, the divergence of the net radiative flux, \mathbf{F}_{rad} , has been rewritten as a net volumic radiative heating rate.

In radiatively-dominated regions of an atmosphere, which is typically the case at and above infrared photospheric levels in hot Jupiter atmospheres (Seager et al. 2005, Cowan & Agol 2011, Menou 2012; Perna et al. 2012), the advective term ($\mathbf{v} \cdot \nabla T$) can be neglected by comparison to the net radiative term (Q_{rad}). Furthermore, near radiative equilibrium, this net radiative term can be expanded into a first-order Taylor series around the local radiative equilibrium temperature, T_{eq} (Goody & Yung 1989), so that the energy equation in a

radiatively-dominated atmosphere reduces to

$$\frac{\partial T}{\partial t} = \frac{T_{\text{eq}} - T}{\tau_{\text{rad}}} + \frac{Q_{\text{ohm}}}{\rho C_p}, \quad (1)$$

where τ_{rad} is the time to relax to radiative equilibrium in this so-called Newtonian approximation. Ohmic dissipation provides a strictly positive contribution, so that in steady-state ($\partial T/\partial t = 0$), one expects thermal balance through net radiative cooling, at an atmospheric temperature $T > T_{\text{eq}}$. This defines the basic radiative-ohmic state on which we wish to perform a stability analysis.

Magnetic Induction Formalism – We use the steady-state axisymmetric magnetic induction framework introduced by Liu et al. (2008) and further discussed in the hot Jupiter context by Batygin & Stevenson (2010), Perna et al. (2010a,b) and Menou (2012). In this framework, a weakly-ionized zonal wind with velocity scale V_ϕ flows across the planetary magnetic field of surface strength B . This induces an additional magnetic field in the atmosphere and, in steady-state, this magnetic induction is balanced by resistive diffusion and associated ohmic dissipation in the atmosphere.

Lacking detailed models for how electric currents flow in the generally inhomogeneous atmospheres of hot Jupiters and other hot exoplanets, we evaluate the heating term associated with ohmic dissipation in Eq. (1) simply as

$$H_{\text{ohm}} \equiv \frac{Q_{\text{ohm}}}{\rho C_p} = \frac{V_\phi^2 B^2}{4\pi\eta\rho C_p} = \frac{V_\phi^2}{\tau_{\text{drag}} C_p}, \quad (2)$$

where η is the electric resistivity and $\tau_{\text{drag}} = 4\pi\eta\rho/B^2$ is the corresponding magnetic drag time. The local electric resistivity of the atmospheric gas is evaluated as $\eta = 230\sqrt{T}/x_e \text{ cm}^2 \text{ s}^{-1}$, where x_e is the free electron ionization fraction (e.g., Menou 2012). This expression for Q_{ohm} , which emerges from simple dimensional analysis of the induction equation (Menou 2012), is consistent with more detailed calculations which find that the bulk of the ohmic dissipation is located in the active weather layer where induction occurs (e.g., Batygin & Stevenson 2010; Perna et al. 2010b; Wu & Lithwick 2012). The exponential dependence of η and Q_{ohm} with temperature when thermal ionization dominates is at the origin of the thermo-resistive instability.

Linear Instability Criterion – Let us denote by C_{rad} the first, radiative relaxation term on the right-hand side of Eq. (1). Radiative-ohmic equilibrium is satisfied when, in Eq. (1), the heating term H_{ohm} (defined in Eq. [2]) exactly balances the cooling term C_{rad} (with $T > T_{\text{eq}}$). This radiative-ohmic thermal equilibrium may be unstable, however, if

$$\frac{dH_{\text{ohm}}}{dT} > -\frac{dC_{\text{rad}}}{dT} = \frac{1}{\tau_{\text{rad}}}, \quad (3)$$

so that a slight temperature increment would lead to a greater increase in ohmic heating than in net radiative cooling. In the limit of weak drag, V_ϕ changes so weakly with temperature, despite the varying magnetic drag (e.g., Menou 2012 or Eq. [3] below), that

$$\frac{dH_{\text{ohm}}}{dT} \simeq \frac{dH_{\text{ohm}}}{d\eta} \frac{d\eta}{dT} = -\frac{H_{\text{ohm}}}{\eta} \frac{d\eta}{dT} \quad (4)$$

To obtain a result in analytic form, we use here a simplified expression for the ionization fraction, which only accounts for potassium ionization (Balbus & Hawley 2000),

$$\begin{aligned} x_e \equiv \frac{n_e}{n_n} &= 6.47 \times 10^{-13} \left(\frac{a_K}{10^{-7}} \right)^{1/2} \left(\frac{T}{10^3} \right)^{3/4} \\ &\times \left(\frac{2.4 \times 10^{15}}{n_n} \right)^{1/2} \frac{\exp(-25188/T)}{1.15 \times 10^{-11}}, \end{aligned} \quad (5)$$

where n_e and n_n are the number densities of electrons and of neutrals, respectively (in cm^{-3}), $a_K = 10^{-7}$ is the potassium abundance (assumed to be solar), and T is the temperature in K. With this expression for x_e , we obtain

$$\begin{aligned} \frac{dH_{\text{ohm}}}{dT} &= H_{\text{ohm}}(2.5 \times 10^{-4} T_3^{-1} + 2.52 \times 10^{-2} T_3^{-2}) \\ &\simeq 4.2 \times 10^{-9} \text{ s}^{-1} \frac{V_{\phi,5}^2 B_1^2 T_3^{1/4}}{\rho^{3/2}} \exp\left(\frac{-25.188}{T_3}\right) [2.5 \times (10^{-4} T_3^{-1} + 10^{-2} T_3^{-2})], \end{aligned} \quad (6)$$

where we adopted $C_p = 1.4 \times 10^8 \text{ erg g}^{-1} \text{ K}^{-1}$, T_3 is the temperature T in units of 1000 K, $V_{\phi,5}$ is the zonal velocity scale V_ϕ in units of km s^{-1} and B_1 is the magnetic field strength in G.

The scaling in Eq. (6) reveals that instability is favored at lower atmospheric densities (hence lower pressures), for larger values of the magnetic field strength and the zonal wind velocity scale, and at higher temperatures ($T \gtrsim 10^3 \text{ K}$), with a strong exponential T -dependence. For conditions representative of the mbar pressure level on the day-side of a hot Jupiter such as HD209458b, $T \sim 1500 \text{ K}$, $\rho \sim 10^{-8} \text{ g cm}^{-3}$, one obtains $dH_{\text{ohm}}/dT \sim 2.9 \times 10^{-3} \text{ s}^{-1}$ for $B = 10 \text{ G}$ and $V_\phi = 3.3 \text{ km s}^{-1}$. By comparison, the radiative relaxation time $\tau_{\text{rad}} \simeq 3 \times 10^3 \text{ s}$ at the mbar level in such an atmosphere (e.g., Showman

et al. 2008), which indicates thermally unstable conditions since $dH_{\text{ohm}}/dT > 1/\tau_{\text{rad}}$. The instability would disappear, however, for lower values of the magnetic field strength ($B \lesssim 1$ G), the wind velocity scale ($V_\phi \lesssim 1$ km s⁻¹) or the atmospheric temperature ($T \lesssim 1000$ K).

This derivation is useful to illustrate the potential for thermal instability and to understand parameter dependencies but it is only valid when magnetic drag is inefficient and when thermal ionization is dominated by potassium. In order to establish more reliable domains of instability, we now relax these assumptions and turn to a numerical parameter space exploration.

3. Thermo-Resistive Instability Domain

Method – Relaxing the weak drag limit implies the need for a magnetic drag law that specifies the magnitude of drag as a function of atmospheric resistivity, η and magnetic field strength, B . In the interest of simplicity, we adopt here a parameterized drag law inspired from the physical arguments developed in Menou (2012). We evaluate the dragged zonal velocity scale, V_ϕ^d , from the drag-free value V_ϕ according to

$$V_\phi^d = \frac{V_\phi}{1 + n_s (V_{\text{drag}}/V_\phi)^{n_e}}, \quad (7)$$

where $V_{\text{drag}} = R_p/\tau_{\text{drag}}$ is a characteristic drag velocity evaluated from the drag time τ_{drag} (previously defined in Eq. [2]) and the planetary radius, R_p . We use the dragged velocity, V_ϕ^d , in all our ohmic dissipation calculations. This formulation satisfies the weak drag expectation $V_\phi^d \rightarrow V_\phi$ at low temperatures (high resistivities) and the strong drag exponential dropoff, $V_\phi^d \propto \eta$ (for $n_e = 1$), expected at high temperatures (e.g Menou 2012). The additional dimensionless parameters n_s and n_e , with default values of unity, are used to control the threshold and the steepness of the transition from the weak to the strong drag regimes. With this drag law, the half-speed transition for a $P = 60$ mbar pressure level (near the thermal photosphere) occurs at a temperature $T \sim 2250$ K for $B = 3$ G, $T \sim 1900$ K for $B = 10$ G and $T \sim 1650$ K for $B = 30$ G, with a half-width $\Delta T \sim 200$ – 300 K. Adopting a weaker drag law, with $n_s = 0.3$ and $n_e = 1$, pushes these transitions to higher temperatures ($T \sim 2500$, 2000 and 1750 K for $B = 3$, 10 and 30 G). While this parameterized magnetic drag law is broadly consistent with the results discussed in Menou (2012), it also clearly is one of our most uncertain model ingredients.

We use here a more detailed, numerical solution to the Saha equation for the thermal ionization fraction x_e (described in Menou 2012), rather than the analytic, potassium-only

formulation discussed in the previous section. This allows us to explore more consistently the low resistivity and high temperature ($T > 1700$ K) regime which is relevant to the hottest exoplanets. Finally, we adopt a zonal velocity profile, with default scale $V_\phi = 7$ km/s (before drag is applied), that decreases exponentially with depth according to $\exp(-P_1)$, where P_1 is the pressure in units of 1 bar. This velocity scale and its rapid decline at high pressures are broadly consistent with the results of Rauscher & Menou (2012) and other published circulation models on the properties of superrotating equatorial winds on hot Jupiters.

We identify instability domains by numerically evaluating the ohmic derivative term dH_{ohm}/dT and comparing it to the inverse of the radiative relaxation time, τ_{rad} . Regions satisfying the inequality in Eq. (2) are considered unstable. We estimate the radiative times on the basis of the work of Iro et al. (2005) and Showman et al. (2008), which yield consistent results for HD209458b. We note that the tabulated, planet-specific values provided by Showman et al. (2008) approximately follow the simple scaling $\tau_{\text{rad}} \propto T^{-3}$ over a wide range of pressures, as may be expected from the formal definition of τ_{rad} (e.g., Goody & Yung 1989). In the interest of generality, we normalize our radiative times to the values found by Iro et al. (2005), using fits provided in Heng et al. (2011), and at each pressure level, we scale the radiative time in proportion to $(T_{\text{iro}}/T)^3$, where $T_{\text{iro}}(P)$ is the corresponding temperature value in the profile of Iro et al. (2005). While this procedure is not expected to yield τ_{rad} values more accurate than a factor of a few, it is sufficient given other sources of uncertainty in our modeling methodology.

Results – Figure 1 presents dayside temperature-pressure profiles for a prototypical hot Jupiter with radius $R_p = 10^{10}$ cm and surface gravity $g = 900$ cm s $^{-2}$. Fifty logarithmically-spaced profiles are shown for values of the planetary effective temperature from $T_{\text{eff}} = 1000$ K to 2500 K. The profiles are calculated with the one-dimensional radiative solution presented by Guillot (2010), for a zero incidence angle and a dilution factor $f = 0.5$ representing a dayside average. An internal heat flux corresponding to $T_{\text{int}} = 150$ K is adopted. As shown by Guillot (2010), even when adopting constant thermal and visible absorption coefficients as is done here ($\kappa_{\text{th}} = 10^{-2}$ cm 2 g $^{-1}$ and $\kappa_{\text{v}} = 4 \times 10^{-3}$ cm 2 g $^{-1}$), these temperature-pressure profiles are reasonably good solutions for hot Jupiter atmospheres over a large range of insolation fluxes. For reference, HD209458b has $T_{\text{eff}} \simeq 1420$ K which corresponds to the twentieth profile from the left.

Thermo-resistive instability domains are also shown in color in Fig. 1 for a default magnetic drag law ($n_s = n_e = 1$ in Eq. [3]). The green and red instability domains correspond to a zonal velocity scale $V_\phi = 7$ km s $^{-1}$ and magnetic field strengths of $B = 10$ and 40 G, respectively. The blue instability domain corresponds to $V_\phi = 10$ km s $^{-1}$ and $B = 3$ G. For $V_\phi = 7$ km s $^{-1}$ and $B = 3$ G no instability is found. As expected, higher velocities

promote instability. Larger magnetic field strengths also promote instability and tend to shift the instability domain to lower atmospheric temperatures. Details of the adopted T-P profiles (e.g., opacity coefficients, dilution factor f) have only minor effects on the instability domains in the sense that instability is primarily set by physical conditions which correspond to specific regions of the T-P plane.

The boundaries of the instability domains, which can be extended in pressure but are typically limited to a narrow range of temperatures, can be understood as follows. To the left of each instability domain, at low temperatures, resistivity varies too weakly with temperature for instability to occur. At the bottom of each instability domain, besides the rapid exponential drop of velocity with pressure, we find that our assumption of a radiatively-dominated atmosphere breaks down. We thus arbitrarily truncated the instability domain at the point where $\tau_{\text{adv}} = R_p/V_\phi = \tau_{\text{rad}}$, with the implicit assumption that strong advective cooling would likely neutralize the instability. More stringent criteria ($\tau_{\text{rad}} \ll \tau_{\text{adv}}$) would further reduce the instability domains to pressure $\lesssim 0.3\text{-}0.1$ bar in all our figures. Finally, to the right and at the top of each instability domain, the emergence of the strong magnetic drag regime rapidly leads to $V_\phi^d \ll V_\phi$ and the effective disappearance of the instability.

Figure 2 shows that a weaker drag law (with $n_s = 0.3$, $n_e = 1$ in Eq. [3]), for the same zonal velocity scale $V_\phi = 7$ km/s and magnetic field strength $B = 10$ G, can result in a significantly more extended instability domain (compare to the green domain in Fig. 1), by pushing the transition to strong drag to higher temperatures. Using $n_e > 1$ in Eq. (3) to steepen the transition to strong drag has only minor effects on the instability domains.

Interestingly, the upper atmosphere of hot Jupiters and other strongly-forced exoplanets are subject to strong photo-ionization rates. An examination of the arguments in section §2 shows that the addition of a temperature-independent contribution to the ionization fraction does not impact the value of dH_{ohm}/dT or the instability criterion. However, the lower resistivity due to the additional ionization results in stronger magnetic drag, which is a limiting factor for the instability. Figure 3 shows the same instability domain as in Fig. 2, when a constant ionization fraction $x_e^+ = 10^{-8}$ is added everywhere in the atmosphere, to emulate the effects of photoionization. This level of additional ionization stabilizes the lowest-density, upper atmospheric regions, where magnetic drag is the strongest. We find that the entire atmospheric domain can be stabilized with the addition of a constant ionization fraction $x_e^+ \sim 10^{-7}$.

Fortney et al. (2003) modeled sodium photoionization in the atmosphere of HD209458b and found ionization fractions in excess of thermal values at pressure levels $\lesssim 30\text{-}100$ mbar, corresponding to $x_e^+ \gtrsim 10^{-8}$ (for a solar abundance of sodium). This, together with the results shown in Fig. 3, suggests that plausible levels of photo-ionization may indeed con-

control the occurrence of the thermo-resistive instability in hot exoplanet atmospheres. At particularly high photo-ionization levels (and possibly super-solar atmospheric abundances), photo-ionization could entirely suppress the instability. Provided one associates the thermo-resistive instability with the observationally-inferred phenomenon of dayside temperature inversions, these results would appear consistent, at least qualitatively, with the observational trend established by Knutson et al. (2010): hot Jupiters subject to the strongest photo-ionization fluxes are the least likely to show such inversions.

4. Discussion and Conclusion

Our argument for the existence of a thermo-resistive instability in the atmospheres of hot, strongly-forced exoplanets relies on a number of assumptions which are not all well justified. Most importantly, the induction formalism used here and in other studies of magnetic effects in hot Jupiter atmospheres and interiors assumes axisymmetry and steadiness. We already emphasized in Perna et al. (2010a) the clearly non-axisymmetric properties of strongly-forced exoplanet atmospheres, a situation that would only be aggravated by the onset of a localized thermal instability (e.g., on the dayside).

Our study of an MHD-based instability with a steady-state induction equation is another important shortcoming. Dimensional analysis of the time-dependent axisymmetric induction equation (see Eq [1] in Menou 2012) suggests that induced currents would lag changes in temperature and resistivity by a resistive diffusion time, $\tau_{\text{diff}} \sim L^2/\eta$. Adopting a pressure scaleheight for the characteristic lengthscale L , we estimate that $\tau_{\text{diff}} < \tau_{\text{rad}}$ for the green and red instability domains in Fig. 1, which suggests that current-adjustment delays will not strongly affect the instability development. At high temperatures and low densities, however, around the blue instability domain and at higher temperatures in Fig. 1, resistivities become small and $\tau_{\text{diff}} > \tau_{\text{rad}}$, which may invalidate the implicit assumption of instantaneous current adjustment made in our steady-state evaluation of the ohmic dissipation term in Eq. (2). A careful consideration of this issue likely requires a full MHD treatment and we shall simply note here that time-dependent current adjustments may impact the thermo-resistive instability of the hottest exoplanet atmospheres beyond the simple treatment adopted here.

Despite such limitations, it is tempting to associate the thermo-resistive instability mechanism identified here with the dayside thermal inversions inferred for a number of hot Jupiters. As shown in Fig. 1, the instability domain is restricted to a specific range of pressures and temperatures. For magnetic field strengths $B \sim 3\text{-}30$ G, instability domains can match well the upper atmospheric dayside conditions of moderately hot exoplanets such as HD209458b, with low enough nightside temperatures $T \lesssim 1100$ K to suppress the insta-

bility. On cooler hot Jupiters such as HD189733b, dayside conditions would barely achieve instability (see T - P profiles in Showman et al. 2008 and Rauscher & Menou 2012). By contrast, very hot exoplanets with $T_{\text{eff}} > 1500$ -2000 K may be too hot on their daysides for instability, and even if their nightsides were to meet the temperature requirements, the instability may be suppressed because of the very effective wind drag exerted on the dayside or possibly strong deviations from radiative equilibrium on the nightside. In principle, some hot exoplanets may be preferentially unstable near their limb, which will be an interesting issue to explore with improved instability models.

The outcome of the instability is difficult to anticipate beyond qualitative expectations. Unstable regions should reach temperatures high enough for saturation of the instability in the strong drag regime, which can amount to temperature excesses of several hundreds Kelvin according to the width of domains shown in Figs. 1–3. Perhaps more importantly, the radiative response of the vertically-coupled atmospheric layers, together with the horizontal coupling caused by locally modified thermal and drag conditions, will result in a very non-linear response that is best studied with global models. While short instability growth times may prove numerically challenging, global circulation models with adequate MHD treatments offer a promising avenue for progress. They would help clarify the global energetics of the instability, which is ultimately powered by the same differential thermal forcing as the global circulation itself.

The author thanks E. Rauscher for comments on the manuscript. This work was supported in part by NASA grant PATM NNX11AD65G.

REFERENCES

- Balbus, S. A., Hawley, J. F. 2000 *Space Science Rev.*, 92, 39
- Baraffe, I., Chabrier, G., Barman, T. 2010, *Reports on Progress in Physics*, Vol. 73, Issue 1, pp. 016901
- Batygin, K. & Stevenson, D. J. 2010, 714, L238
- Batygin, K., Stevenson, D. J. & Bodenheimer, P. H. 2011, *ApJ* 738, 1
- Burrows, A., Budaj, J. & Hubeny, I. 2008, *ApJ* 678, 1436
- Burrows, A. & Orton, G. 2010, in “Exoplanets”, *Space Science Series of the University of Arizona Press* (Tucson, AZ); Ed. S. Seager; arXiv:0910.0248
- Charbonneau, D. 2009, in “Transiting Planets”, *Proceedings of the International Astronomical Union, IAU Symposium, Volume 253*, p. 1-8

- Cowan, N. B. & Agol, E. 2011, *ApJ* 729, 54
- Deming, D. & Seager, S. 2009, *Nature* 462, 301
- Fortney, J. J., Sudarsky, D., Hubeny, I. et al. 2003, *ApJ* 589, 615
- Fortney, J. J., Saumon, D., Marley, M. S., Lodders, K., & Freedman, R. S. 2006, *ApJ*, 642, 495
- Fortney, J. J., Lodders, K., Marley, M. S., & Freedman, R. S. 2008, *ApJ*, 678, 1419
- Guillot, T. 2010, *A&A* 520, A27
- Goody, R. M. & Yung, Y. L. 1989, *Atmospheric radiation : theoretical basis*. 2nd ed, New York, NY: Oxford University Press
- Heng, K., Menou, K. & Phillipps, P. J. 2011, *MNRAS* 413, 2380
- Iro, N., Bezar, B. & Guillot, T 2005, *A&A*, 436, 719
- Knutson, H. A., Howard, A. W. & Isaacson, H. 2010, *ApJ* 720, 1569
- Hubeny, I., Burrows, A., & Sudarsky, D. 2003, *ApJ*, 594, 1011
- Laughlin, G., Crismani, M. & Adams, F. C. 2011, *ApJ* 729, L7
- Liu, J., Goldreich, P. M., & Stevenson, D. J. 2008, *Icar.*, 653, 664
- Madhusudhan, N. & Seager, S. 2010, *ApJ* 725, 261
- Menou K. 2012, *ApJ* 745, 138
- Perna, R., Heng, K. & Pont, F. 2012, *ApJ* 751, 59
- Perna, R., Menou, K. & Rauscher, E., 2010a, *ApJ* 719, 1421
- Perna, R., Menou, K. & Rauscher, E., 2010b, *ApJ* 724, 313
- Rauscher, E. & Menou, K. 2012, *ApJ* 750, 96
- Seager, S., Richardson, L. J., Hansen, B. M. S., Menou, K., Cho, J. Y.-K. & Deming, D. 2005, *ApJ* 632, 112
- Showman, A. P., Cooper, C. S., Fortney, J. J., & Marley, M. S. 2008, *ApJ*, 682, 559
- Winn, J. 2010, in “Exoplanets”, Space Science Series of the University of Arizona Press (Tucson, AZ); Ed. S. Seager; arXiv:1001.2010
- Wu, Y. & Lithwick, Y. 2012, *ApJ* submitted, arXiv:1202.0026

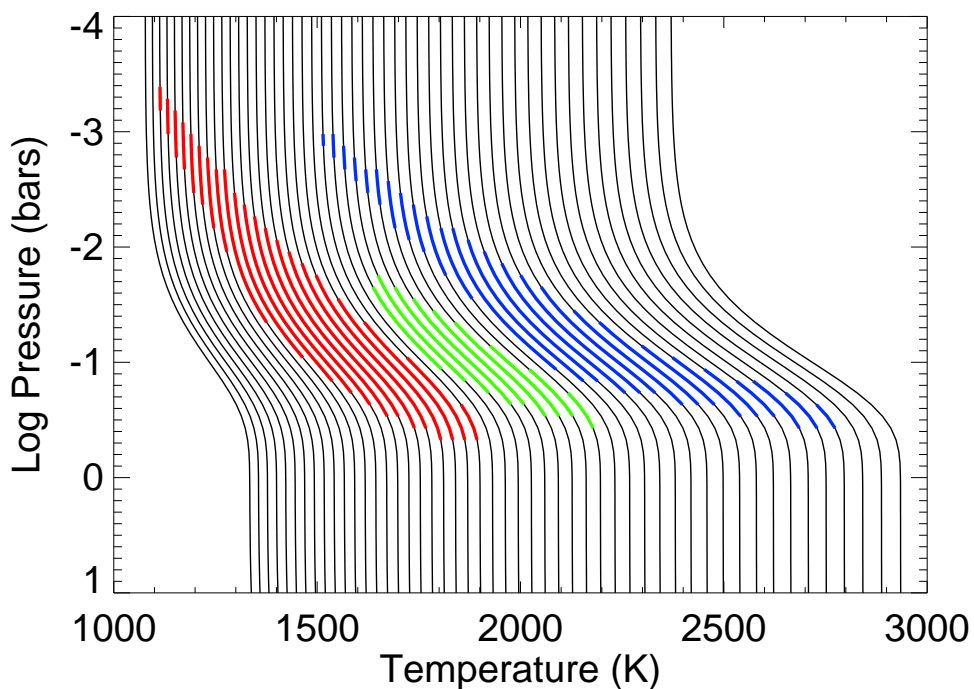


Fig. 1.— Thermo-resistive instability domains superposed on temperature-pressure profiles representative of the dayside of a typical hot Jupiter, for the default magnetic drag law ($n_s = n_e = 1$ in Eq. [3]). The green and red instability domains correspond to a zonal velocity scale $V_\phi = 7 \text{ km s}^{-1}$ and magnetic field strengths $B = 10$ and 40 G , respectively. The blue instability domain corresponds to $V_\phi = 10 \text{ km s}^{-1}$ and $B = 3 \text{ G}$.

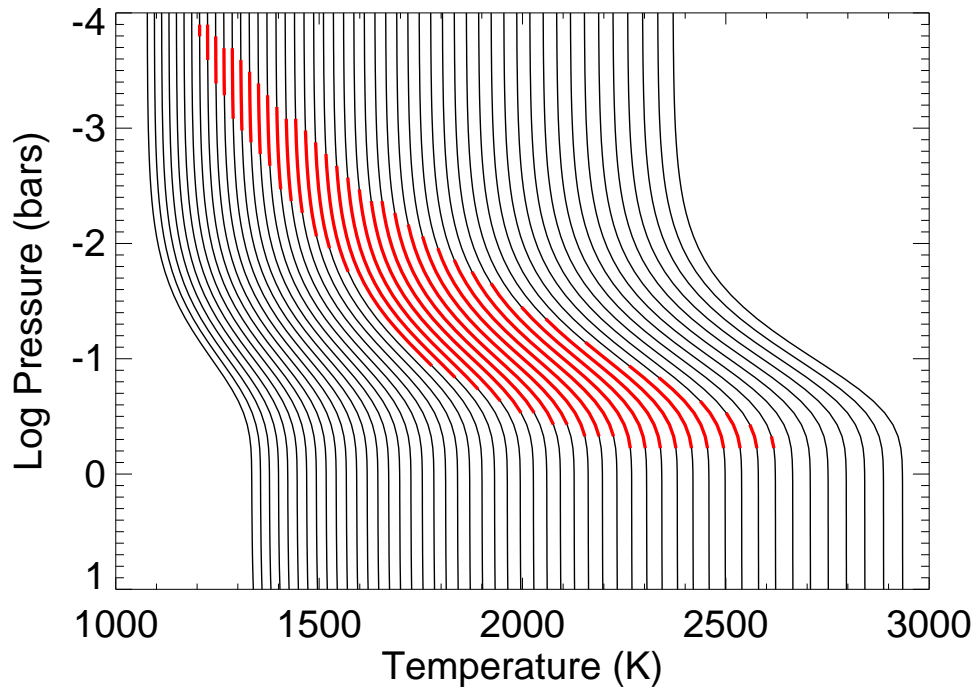


Fig. 2.— Same as Figure 1 with a weaker magnetic drag law ($n_s = 0.3$, $n_e = 1$ in Eq. [3]), $V_\phi = 7 \text{ km s}^{-1}$ and $B = 10 \text{ G}$. This drag law delays the transition into the strong drag regime to higher temperatures, which extends the domain of instability (compare to the green domain in Figure 1).

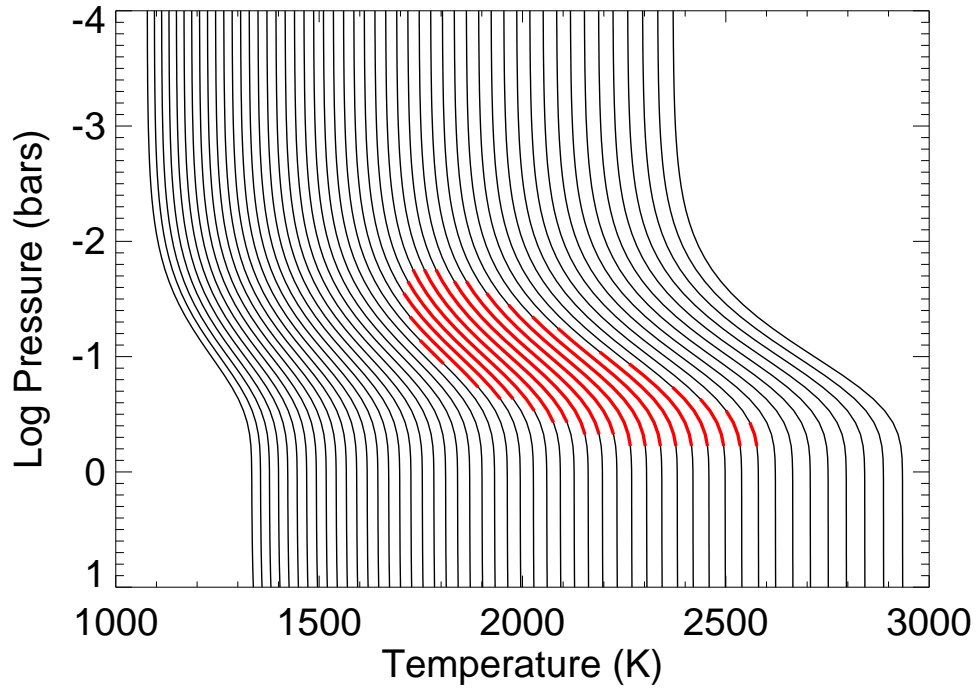


Fig. 3.— Same as Figure 2 with a constant ionization fraction $x_e^+ = 10^{-8}$ added throughout the atmosphere, to mimick the effects of photoionization. The additional, constant ionization contribution stabilizes the upper atmospheric regions by inducing a stronger drag regime. The entire atmospheric domain can be stabilized with the addition of a constant ionization fraction $x_e^+ \sim 10^{-7}$.